



**HAL**  
open science

## Sulfur Isotope Anomalies ( $\Delta 33\text{ S}$ ) in Urban Air Pollution Linked to Mineral-Dust-Associated Sulfate

Sanjeev Dasari, Guillaume Paris, Bruna Saar, Qiaomin Pei, Zhiyuan Cong,  
David Widory

► **To cite this version:**

Sanjeev Dasari, Guillaume Paris, Bruna Saar, Qiaomin Pei, Zhiyuan Cong, et al.. Sulfur Isotope Anomalies ( $\Delta 33\text{ S}$ ) in Urban Air Pollution Linked to Mineral-Dust-Associated Sulfate. *Environmental Science and Technology Letters*, 2022, 9 (7), pp.604-610. 10.1021/acs.estlett.2c00312 . hal-03758312

**HAL Id: hal-03758312**

**<https://hal.science/hal-03758312>**

Submitted on 23 Aug 2022

**HAL** is a multi-disciplinary open access archive for the deposit and dissemination of scientific research documents, whether they are published or not. The documents may come from teaching and research institutions in France or abroad, or from public or private research centers.

L'archive ouverte pluridisciplinaire **HAL**, est destinée au dépôt et à la diffusion de documents scientifiques de niveau recherche, publiés ou non, émanant des établissements d'enseignement et de recherche français ou étrangers, des laboratoires publics ou privés.

1 SO<sub>2</sub> photo-oxidation on mineral dust: The missing link to  
2 explain  $\Delta^{33}\text{S}$  anomalies in urban sulfate aerosols

3 Sanjeev Dasari<sup>1\*</sup>, Guillaume Paris<sup>2</sup>, Bruna Saar<sup>3</sup>, Qiaomin Pei<sup>4</sup>,  
4 Zhiyuan Cong<sup>4</sup>, David Widory<sup>3\*</sup>

5  
6 <sup>1</sup>Institut des Géosciences de l'Environnement (IGE), Université Grenoble Alpes, CNRS, IRD,  
7 Grenoble INP, Grenoble 38000, France

8 <sup>2</sup>Université de Lorraine, CRPG, CNRS, Vandœuvre-lès-Nancy 54500, France

9 <sup>3</sup>GEOTOP/ Université du Québec à Montréal, Montréal H3C 3P8, Canada

10 <sup>4</sup>Key Laboratory of Tibetan Environment Changes and Land Surface Processes,  
11 Institute of Tibetan Plateau Research, Chinese Academy of Sciences, Beijing 100101, China

12

13 **KEYWORDS**

14 Sulfur Mass-Independent Fractionation (S-MIF), UV radiation, Air Pollution, Particulate Matter,  
15 Model-Observation Reconciliation

16 **ABSTRACT**

17 Sulfate aerosols exert a net cooling effect on the earth-atmosphere system, yet their radiative  
18 forcing remains associated with largest of uncertainties in the assessment of climate change. One  
19 of the contributing factors is the poor understanding of the sulfate formation pathways, which are  
20 thought to be following mostly the mass-dependent fractionation model (i.e.,  $\Delta^{33}\text{S} \sim 0$ ). However,  
21 globally, urban sulfate aerosols exhibit significant non-zero  $\Delta^{33}\text{S}$  compositions (from -0.6‰ to  
22 +0.6‰), resulting in sulfur mass-independent fractionation (S-MIF) processes. The origin(s) of  
23 these S-MIF anomalies remain(s) unclear. Here, we conducted dual-isotope ( $\Delta^{33}\text{S}$ ,  $\delta^{34}\text{S}$ ) probing  
24 of sulfate aerosols from summertime megacity Delhi in South Asia. A shift towards concomitantly  
25 high  $\Delta^{33}\text{S}$  (from +0.2‰ to +0.5‰) and low  $\delta^{34}\text{S}$  (from +5‰ to +1‰) values was observed with  
26 the influx of mineral dust. The Fe-to-Al tracer showed significant correlations with sulfate loadings  
27 ( $R^2=0.84$ ) and  $\Delta^{33}\text{S}$  signatures ( $R^2=0.77$ ). As such, we postulate that the  $\text{SO}_2$  photo-oxidation on  
28 mineral dust generates S-MIF anomaly  $\sim +0.35 \pm 0.10$ ‰, thereby also explaining the previously  
29 observed  $\Delta^{33}\text{S}$  values worldwide. Together, the findings help deconvolute S-isotope dynamics in  
30 urban regions wherein, contrary to prevailing paradigm, non-anthropogenic factor (i.e., mineral  
31 dust) is found to influence the aerosol sulfate-induced pollution affecting air quality/human health.

32 **SYNOPSIS**

33 Sulfate-related pollution in urban regions—affecting air quality/human health—could be linked to  
34 non-anthropogenic factor i.e., mineral dust.

## 35 INTRODUCTION

36 Sulfur (S) is one of the essential elements for life. The sulfur biogeochemical cycle  
37 contributes to controlling the redox state of Earth's surface and links the atmosphere, biosphere,  
38 hydrosphere, and the lithosphere<sup>1</sup>. Yet, the sulfur cycle is massively disrupted by human activities<sup>1-  
39 3</sup>. The majority of natural and anthropogenic S is released directly as SO<sub>2</sub> (gas) or oxidized into  
40 SO<sub>2</sub> in the atmosphere<sup>2</sup>. On a global scale, ~50% of SO<sub>2</sub> (natural and anthropogenically emitted)  
41 is oxidized to sulfate while the rest is lost to dry and wet scavenging<sup>3</sup>. The pathway taken by SO<sub>2</sub>  
42 to form sulfate has major implications for both the radiative effects and the environment— in gas-  
43 phase reactions occurring predominantly with hydroxyl radicals (OH), the end-product sulfuric  
44 acid (g) leads to new particle formations eventually altering the cloud albedo and lifetime<sup>4</sup>. In the  
45 heterogenous phase reactions occurring primarily in cloud droplets via several oxidants, the major  
46 ones being O<sub>2</sub>+TMI (Transition Metal Ion), H<sub>2</sub>O<sub>2</sub>, O<sub>3</sub> and NO<sub>2</sub>, the end-product sulfate particles  
47 contribute towards modifying the aerosol size distribution and cloud condensation nuclei activity<sup>5</sup>.  
48 On a global scale, the sulfate aerosols contribute to a negative effective radiative forcing (ERF) of  
49 -0.90 (-0.24 to -1.56) W m<sup>-2</sup> (IPCC, 2021). As such, the net cooling effect of sulfate aerosols  
50 partially counteracts the warming effects of greenhouse gases (e.g., CO<sub>2</sub>, CH<sub>4</sub>)<sup>3,6</sup>. However, the  
51 magnitude and expected future changes in sulfate aerosol radiative forcing remains one of the  
52 largest uncertainties associated with assessments of climate change<sup>6</sup>.

53 To this end, S-isotope geochemistry can be used towards addressing these uncertainties as  
54 it provides powerful information for deconvolution of both emission sources and atmospheric  
55 processes<sup>7-9</sup>. Sulfur has four stable isotopes, <sup>32</sup>S, <sup>33</sup>S, <sup>34</sup>S and <sup>36</sup>S whose natural abundances are  
56 approximately 95%, 0.75%, 4.2% and 0.015%, respectively<sup>10,11</sup>. The S-stable isotopes undergo  
57 fractionation during kinetic and equilibrium reactions which causes the reactant (SO<sub>2</sub>) and the

58 product (sulfate) to have distinct isotope compositions<sup>12,13</sup>. In general, the isotope ratios of any two  
59 isotopes can be scaled to each other based on the mass i.e., “mass dependent fractionation (MDF)”  
60 model<sup>9</sup>. More specifically, the fractionation factors determined for MDF processes follow a  
61 relation  $^{3y}a = (^{34}a)^{3yb}$  wherein  $^{3y}a$  could be  $^{33}a$  or  $^{36}a$  and  $^{3y}b$  is  $^{33}b$  or  $^{36}b$  and the  $3yb$  is the relative  
62 fractionation of  $^{3y}S/^{32}S$  and  $^{34}S/^{32}S$ <sup>13</sup>. The  $^{33}b$  and  $^{36}b$  values were experimentally determined to be  
63 0.515 and 1.889<sup>14</sup>. Any deviation from this relationship implies the occurrence of “Mass  
64 Independent Fractionation (MIF)”<sup>15</sup>. The S-MIF is expressed as  $\Delta^{33}S = (\delta^{33}S+1) - (\delta^{34}S+1)^{0.515}$   
65 and  $\Delta^{36}S = (\delta^{36}S+1) - (\delta^{34}S+1)^{1.889}$ . Considerable debate exists in the interpretation of S-MIF  
66 signals observed in atmospheric aerosols from urban locations<sup>e.g.,16-18</sup>.

67 The origin of S-MIF in nature has been primarily attributed to photochemical reactions in  
68 the presence of UV radiation —SO<sub>2</sub> absorption at 190-220 nm i.e., photolysis, and SO<sub>2</sub> absorption  
69 at 250-330 nm i.e., photo-oxidation<sup>15</sup>. These mechanisms have been suggested to account for the  
70 S-MIF observed in the Archean sediments as well as in modern aerosols<sup>15,17</sup>. However, to date the  
71 reported S-MIF values ranging from -0.6‰ to +0.6‰ evidenced in urban aerosols from polluted  
72 regions (e.g., Beijing, Montreal; Supporting Information (SI) Figure S1) have not been fully  
73 explicable with the S-isotope variations in emission sources (e.g., biomass or fossil fuel  
74 combustion with  $\Delta^{33}S$  upto  $\sim \pm 0.2\%$ ) or atmospheric oxidation processes (e.g., homogenous and  
75 heterogenous reactions displaying  $\Delta^{33}S \sim 0\%$ )<sup>16-18</sup>. While a stratospheric origin of sulfate aerosols  
76 has been conceived to perpetuate  $\Delta^{33}S$  in urban aerosols<sup>17</sup>, this is not the case for all locations and  
77 cannot fully resolve the signals reported worldwide<sup>16</sup>. Taken together, this invokes the necessity  
78 for additional oxidation pathways or reactions to be identified for the conversion of SO<sub>2</sub> to sulfate  
79 affecting the  $\Delta^{33}S$  in atmospheric aerosols<sup>16</sup>. As such, it could be a contributing factor for the  
80 uncertainties associated with the radiative forcing of sulfate aerosols on a global scale, and

81 especially in one of the most polluted regions of the world with rising SO<sub>2</sub> levels i.e., S Asia<sup>19</sup>. We  
82 therefore conducted dual-isotope fingerprinting ( $\Delta^{33}\text{S}$ ,  $\delta^{34}\text{S}$ ) of ambient sulfate aerosols in  
83 summertime megacity Delhi in S Asia. Combining chemical, isotopic, and meteorological  
84 information enabled resolving the origin of S-MIF anomalies in one of the most polluted regions  
85 in the world.

86

## 87 **MATERIALS AND METHODS**

88 **Sampling.** Aerosol PM<sub>10</sub> samples (n=44) were collected using an Envirotech Air Pollution  
89 Monitoring 550 aerosol sampler, operated at 1 m<sup>3</sup> hr<sup>-1</sup> with a sampling duration of 24 hours  
90 (sample collection started at 6 am and continued till 6 am of the next day; see SI Table S1). Sample  
91 collection was made between April-May 2021 atop a five-storey residential building in the Anand  
92 Vihar area of Delhi. The area is surrounded by parks and greenery. The sampling period covers  
93 the summer season. Delhi has a semi-arid climate and summer temperatures are on average 45±3  
94 °C<sup>20</sup>. Aerosol samples were collected on pre-combusted (450 °C for 6 h) PALLFLEX tissue quartz  
95 filters (25 cm×20 cm). Filter blanks were collected approximately three times per month. Samples  
96 were stored in a freezer at -20 °C prior to analysis.

97 **Chemical and Isotope Measurements.** The concentration of water-soluble ions and metals, as  
98 well as the S-isotope compositions were measured using an ion chromatography Metrohm IC  
99 (Professional 850) and QQQ-ICP-MS, and a MC-ICP-MS instrument respectively. Measurements  
100 were carried out at the University of Tours (for water-soluble ions) and Centre de Recherches  
101 Pétrographiques et Géochimiques, CRPG (for S-isotopes) in France, and the Université du Québec  
102 à Montréal, UQAM (for metals) in Canada, respectively. Further details on the procedure,

103 measurements, analytical uncertainties, quality control and reproducibility are provided in SI Note  
104 S1.

105

## 106 **RESULTS AND DISCUSSION**

107 **Summertime aerosol characteristics and multi-S-isotope compositions in S Asia.** The  
108 megacity Delhi—located in the heart of the Indo-Gangetic Plain—suffers from acute air pollution  
109 crisis<sup>20</sup>. High average PM<sub>10</sub> concentrations were found during the study period, 90±30 µg/m<sup>3</sup> in  
110 the months of April and 200±80 µg/m<sup>3</sup> in May 2021 (SI Table SI ). This is attributable in general  
111 to features such as several types of anthropogenic activities, collocated emission sources, location  
112 and topography, population density, and socio-economic development<sup>20-22</sup>. Furthermore, long-  
113 range transport of dust from the adjoining Thar Desert and Arabian regions is also known to  
114 contribute towards episodic dust storms and high PM levels during summer<sup>20</sup>.

115 The water-soluble inorganic ions (e.g., SO<sub>4</sub><sup>2-</sup>, K<sup>+</sup>) together contributing as much as 50% to  
116 the PM<sub>10</sub> concentrations serve as tracers for combustion sources and secondary formation  
117 processes<sup>20-23</sup>. Concentrations of one such component, aerosol sulfate, ranged from 1 to 23 µg/m<sup>3</sup>  
118 (Figure 1a) implying a fractional contribution of upto 20% in the PM<sub>10</sub> aerosols. The multi-S  
119 isotope compositions from Delhi ranged from 0.5‰ to 5‰ for δ<sup>34</sup>S, from 0.2‰ to 0.5‰ for Δ<sup>33</sup>S  
120 during summer of 2021 (SI Table S2). In contrast to the observations of low Δ<sup>33</sup>S (< 0.1‰) in the  
121 city of Montreal and high Δ<sup>33</sup>S (~0.5‰) in its corresponding sub-rural background<sup>16</sup>, here we find  
122 such higher values in the city. This however is in accordance with the finding from Beijing (i.e., E  
123 Asia) where a gradient shifting from ~0‰ to positive Δ<sup>33</sup>S values (~0.5‰) has been reported  
124 during the summer<sup>16,17,23</sup>. For δ<sup>34</sup>S, the values are in general lower than those reported for Montreal

125 and Beijing during summer<sup>16,23</sup>, with values lower than 1‰ also being encountered in Delhi during  
126 the latter part of the summer. A shift towards concomitantly high  $\Delta^{33}\text{S}$  and low  $\delta^{34}\text{S}$  values was  
127 observed with proceeding of the summer season (Figure 1a) and could be driven by change in the  
128 sources and/or atmospheric processes.

129 **Evaluation of plausible factors contributing to the sulfate  $\Delta^{33}\text{S}$  dynamics.** The measurements  
130 of multiple S-isotope composition reported here constitute the first for S Asia. The span of the  
131  $\Delta^{33}\text{S}$  values in the present study is such that it cannot be explained by the model proposed by Harris  
132 et al. (2013). Their model, relying upon the seasonal isotope variations induced by three major  
133 oxidation pathways (OH, H<sub>2</sub>O<sub>2</sub>, O<sub>2</sub>+TMI), accounts for a maximum  $\Delta^{33}\text{S}$ -value of 0.05‰ during  
134 summer<sup>18</sup>. This implies that the additional  $\Delta^{33}\text{S}$  dynamics observed in summertime Delhi could  
135 either be linked to changes in origin and/or possibly other chemical reactions.

136 The anthropogenic emission sources could modulate the  $\Delta^{33}\text{S}$  values<sup>17,23,24</sup>. In particular,  
137 biomass burning and/or biofuel combustion have been shown to affect the urban  $\Delta^{33}\text{S}$  signatures<sup>23</sup>.  
138 However, for the summer samples, a poor correlation was found between  $\Delta^{33}\text{S}$  and K<sup>+</sup> (a tracer for  
139 biomass burning) (SI Figure S2). Coal combustion was found to be a large source of aerosol sulfate  
140 in Delhi based on source-apportionment using  $\delta^{34}\text{S}$  (see SI Note S2), however, lab-based studies  
141 have shown both SO<sub>2</sub> and sulfate formed from coal combustion do not carry any  $\Delta^{33}\text{S}$ <sup>17</sup>. Iron  
142 extraction from Archean banded-iron formation (BIF) is another source of atmospheric S that  
143 produces non-zero  $\Delta^{33}\text{S}$ <sup>16</sup>. However, no such activities exist in and around the city<sup>20,21</sup>. Taken  
144 together this suggests that anthropogenic activities do not cause the observed  $\Delta^{33}\text{S}$  isotope  
145 anomalies.

146 Stratospheric intrusions have been implicated for the  $\Delta^{33}\text{S}$  observed in urban aerosols<sup>17</sup>.  
147 However, HYSPLIT model-based back trajectories do not show air masses arriving from the upper



148 troposphere (> 10-15 km) to the sampling location (SI Figure S3). This is consistent with the study  
149 of Lin et al. (2016) who also estimated a very low (< 1%) input of stratospheric SO<sub>4</sub> in their study<sup>25</sup>.  
150 Even with such an input only upto +0.1‰ of the Δ<sup>33</sup>S anomaly may be explained, but not the entire  
151 range witnessed here. Furthermore, such intrusions are more common during the monsoon season  
152 than during the summer season in the Indian sub-continent<sup>26</sup>, which is further corroborated by the  
153 low cloud optical thickness and high cloud top pressure measurements during the summer of 2021  
154 at Delhi (SI Figure S4). We therefore turn our attention to the possibility of chemical reactions/  
155 mechanisms in order to explain the origin of the Δ<sup>33</sup>S values observed in our sulfate aerosols.

156 **Linking chemical and dual S-isotope signals to deconvolute sulfate formation.** Recently, the  
157 role of mineral dust in the formation of secondary aerosol sulfate has been called into contention<sup>16</sup>.  
158 The mechanisms behind the formation of secondary aerosol sulfate mediated by mineral dust  
159 remain elusive<sup>16,27</sup>. For instance, they may include oxidation of SO<sub>2</sub> by the superoxide radical  
160 anion formed on semi-conducting metal oxides like Al<sub>2</sub>O<sub>3</sub>, Fe<sub>2</sub>O<sub>3</sub> and TiO<sub>2</sub> by UV radiation,  
161 oxidation by NO<sub>2</sub><sup>16</sup>. Interestingly, our chemical analyses indicate significant contributions of  
162 mineral dust in the PM<sub>10</sub> aerosols in Delhi as samples present Fe/Al ratios (i.e., the conventional  
163 reference for upper continental crust)<sup>28,29</sup> from as low as 0.2 during April to as high as 1.4 during  
164 May (all > 0.05; Figure 1a), similar to the ones characterizing desert dusts (from 0.48 to 1.74)<sup>29</sup>.  
165 We elected to discuss the Fe/Al ratio which is more representative of mineral dust than the Ca<sup>2+</sup>/Al  
166 ratio, mainly a tracer for carbonate mineral<sup>28,29</sup>.

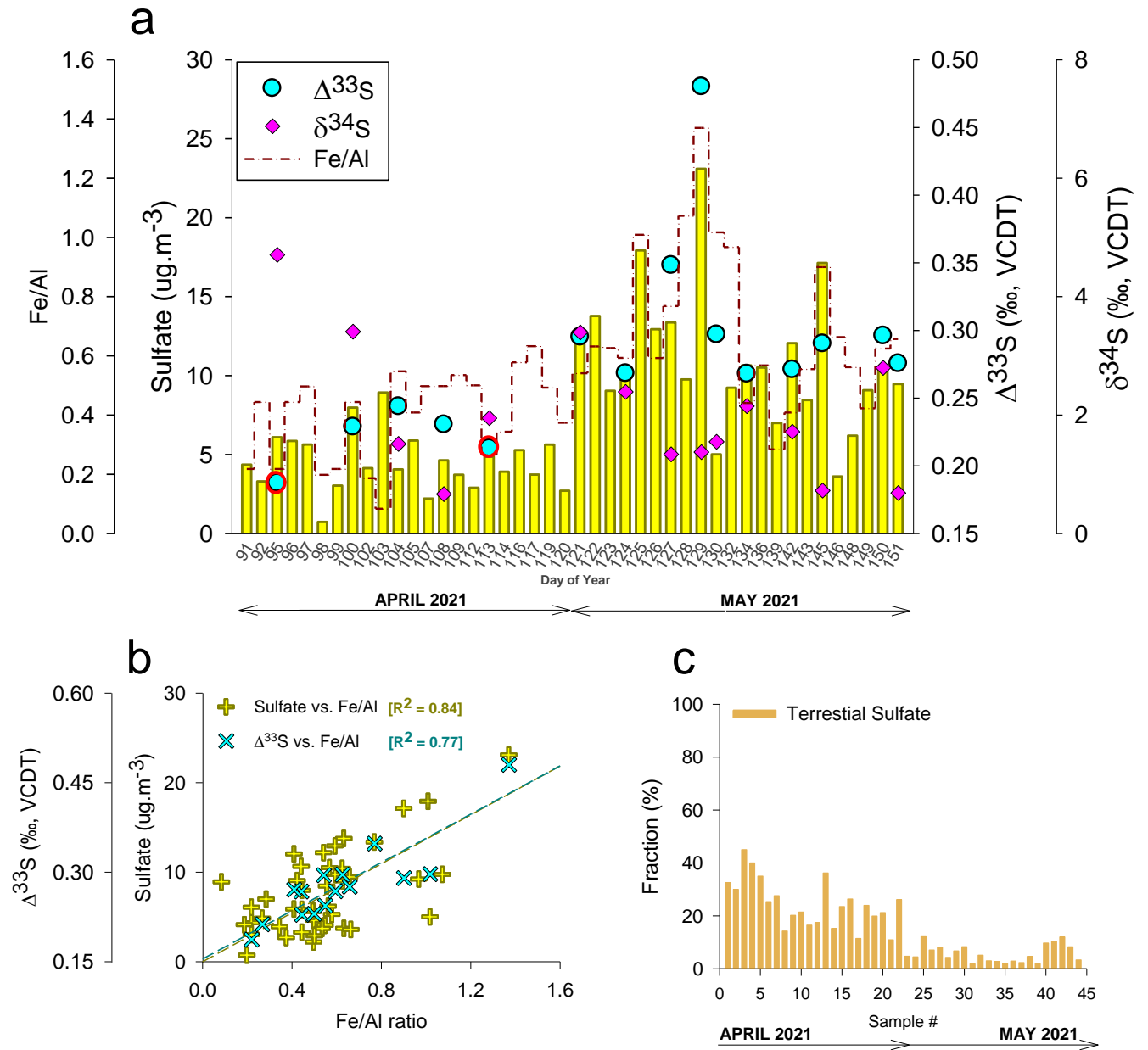
167 Higher Fe/Al ratios were observed with the progression of the summer season concomitant  
168 with the influx of mineral dust from the Thar desert in western India, as evidenced by air mass  
169 analysis and satellite data (SI Figures S3, S5). We find strong correlations between the Fe/Al ratios  
170 and the sulfate loadings (R<sup>2</sup>=0.84) and Δ<sup>33</sup>S values (R<sup>2</sup>=0.77) respectively, highlighting a potential

171 link between the sulfate formation, S-isotope variations and mechanisms involving mineral dust.  
172 In fact, the higher  $\Delta^{33}\text{S}$  anomalies ( $> 0.2\text{‰}$ ) observed in the month of May were concomitant with  
173 5-times higher loadings of mineral dust relative to those of April 2021. Taken together, this implies  
174 that the low  $\Delta^{33}\text{S}$  values ( $< 0.2\text{‰}$ ) are indeed not greatly affected by mineral dust contribution and  
175 can be explained as arising from a combination of different sources/origins and other homogenous  
176 and heterogenous oxidation pathways (upto  $\sim +0.20\text{‰}$ ) or even stratospheric intrusions<sup>17,18,23</sup>. But  
177 the higher  $\Delta^{33}\text{S}$  values (as well as sulfate concentrations) observed in Delhi during summer of 2021  
178 were strongly modulated by the presence of mineral dust.

179 Weak winds combined with a shallow boundary layer can lead to the contribution of high  
180 fine mode resuspended road dust (whose composition remains unknown). This has been observed  
181 in E Asia during the haze episodes<sup>30</sup>. However, such meteorological conditions are more  
182 favourable for wintertime S Asia than summer<sup>20,22</sup>. The terrigenous sulfate source fraction ( $f_{\text{ter-S}}$ )  
183 is useful for accounting the contribution of local resuspended dust (from within the city). Here,  
184 based on ratio of  $\text{SO}_4^{2-}$ -to- $\text{Ca}^{2+}$  concentrations in regional soil to the same in sampled aerosol, we  
185 accounted for the  $f_{\text{ter-S}}$  in summertime Delhi samples (Figure 1c; see also Note S2). We find that  
186 the  $f_{\text{ter-S}}$  decreased from  $20\pm 5\%$  on average in April to  $< 5\pm 2\%$  during May of 2021. This decrease  
187 in  $f_{\text{ter-S}}$  is concomitant with the increase in the Fe-to-Al ratio. This implies that influx of mineral  
188 dust from nearby desert region in W India modulated the formation of aerosol sulfate and thereby  
189 the observed high  $\Delta^{33}\text{S}$  values (as desert dust carries no S-MIF)<sup>16</sup> as the summer progressed. This  
190 also points to the fact that the  $\delta^{34}\text{S}$  signature of mineral dust from the Thar desert might be slightly  
191 lower than that from deserts in China, Morocco, Tunisia and Jordan, with  $\delta^{34}\text{S}$  ranges between 5  
192 and  $13\text{‰}$ <sup>16</sup>.

193 **Implications of mineral dust on sulfate-induced urban air pollution.** Overall, the present  
194 findings suggest that  $\Delta^{33}\text{S}$  is a reliable tracer for better constraining the formation of sulfate  
195 aerosols in the presence of mineral dust. Comparing with previous observations from a sub-rural  
196 background site in Montreal (referred to as station 98 in Au Yang et al., 2019), we find overlapping  
197 characteristics in both  $\Delta^{33}\text{S}$  and  $\delta^{34}\text{S}$  (Figure 2). Here, we conjecture that the high  $\Delta^{33}\text{S}$  values  
198 recorded at station 98 are indeed explicable by the  $\text{SO}_2$  photo-oxidation on mineral dust pathway  
199 in line with the hypothesis by Au Yang et al. . Furthermore, with an estimated  $\Delta^{33}\text{S}$  fingerprint of  
200  $+0.35\pm 0.10\text{‰}$  for this pathway, we are able to also explain the  $\Delta^{33}\text{S}$  values previously observed in  
201 other urban locations such as in E Asia (Figure 2) hinting at a plausible global significance of this  
202 pathway. The implications of the findings here are twofold (i) even a small contribution from  
203 mineral dust-mediated  $\text{SO}_2$  photo-oxidation may have a large effect on the observed  $\Delta^{33}\text{S}$  signals  
204 in aerosols, (ii) regions with low  $\text{SO}_2$  production but high input of mineral dust e.g., remote oceanic  
205 regions<sup>22</sup>, can still act as emission regions of sulfate aerosols, thereby affecting the aerosol  
206 radiative forcing. It remains to be seen if this pathway sustains during vertical transport of  $\text{SO}_2$   
207 where competing mechanisms such as aqueous phase oxidation and/or stratospheric intrusions  
208 become more relevant<sup>31</sup>.

209 For South Asia, the rising  $\text{SO}_2$  levels present a threat to several of the sustainable  
210 development goals for the region such as access to clean air and freshwater<sup>32,33</sup>. For accurate  
211 predictions of future scenarios of the influence of  $\text{SO}_2$  on the region it is imperative to account for  
212 all sources and formation pathways of sulfate. We therefore consider that the findings here would  
213 aid in that direction and contribute towards reducing the model-observation discrepancies in  
214 modeling global and regional sulfate aerosol dynamics wherein the sensitivity of the simulations  
215 remains highly dependent on the accounted oxidation pathways<sup>34</sup>.



217

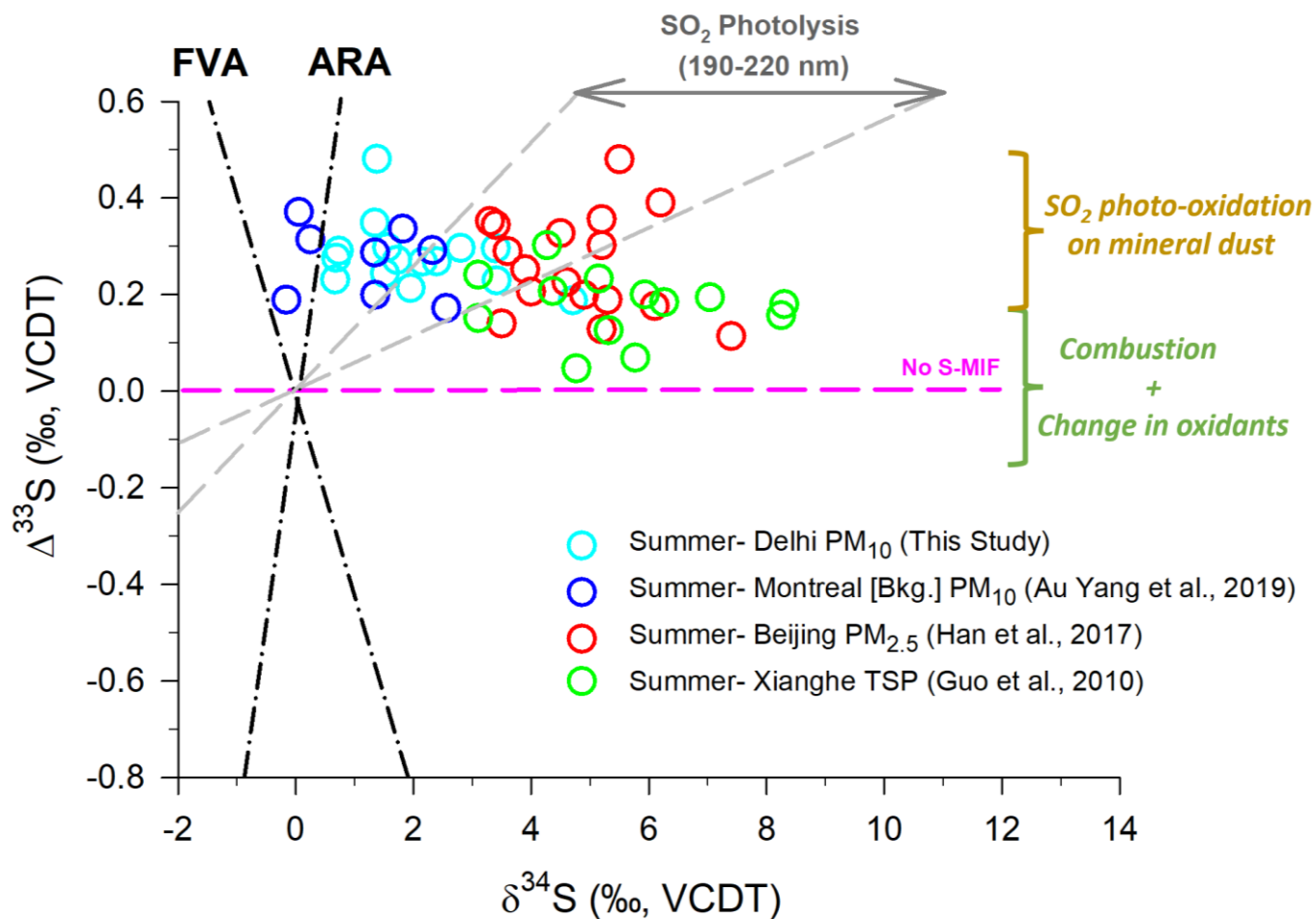
218

219 **Figure 1.** (A) Temporal changes in the sulfate concentrations,  $\Delta^{33}\text{S}$ ,  $\delta^{34}\text{S}$  and Fe/Al ratios,

220 (B) Correlation of the  $\Delta^{33}\text{S}$  signals, sulfate loadings with the influx of mineral dust (see also, SI

221 Table S1-S2, SI Figures S3-S5), (C) Calculated terrestrial sulfate fraction in the PM<sub>10</sub> samples (see

222 also SI Note S2). Samples with red circles (Day 95, 113) refer to the ones collected only during  
223 the nighttime (6 pm to 6 am). As such, these were restricted to 12 h collections.



224

225

226 **Figure 2.** Relation between  $\Delta^{33}\text{S}$  and  $\delta^{34}\text{S}$  for sulfate in Delhi PM<sub>10</sub> during sampling and their  
 227 comparison with aerosols collected from Beijing<sup>23</sup> and Xianghe in E Asia<sup>35</sup> and sub-rural  
 228 background site in Montreal, Canada<sup>16</sup>. ARA represents the Archean Reference Array based on  
 229 the data from Neoproterozoic and Paleoproterozoic rocks in Australia and Africa<sup>36</sup>. FVA represents the  
 230 felsic volcanic array<sup>37</sup>. The gray field represents experiment data from SO<sub>2</sub> photolysis in the  
 231 190–220 nm region (Xenon arc lamp)<sup>15</sup>.

232 **ASSOCIATED CONTENT**

233 **Supporting Information.** Notes S1-S2 include discussions on the chemical and isotope  
234 measurements, source apportionment calculations. Figures S1-S5 include air mass analysis,  
235 satellite data-derived maps, correlations. Tables S1-S2 list the sampling details and concentrations  
236 of water-soluble ions, metals, and multiple S-isotope compositions.

237 **AUTHOR INFORMATION**

238 **Corresponding Authors**

239 \* E-mail: [sanjeev.dasari@univ-grenoble-alpes.fr](mailto:sanjeev.dasari@univ-grenoble-alpes.fr) ; [widory.david@uqam.ca](mailto:widory.david@uqam.ca)

240 Phone: +33 068 564 42 84 ; +1 438 998 11 13

241 **Author Contributions**

242 S.D. designed research and was supported by D.W., Z.C and G.P.; S.D., B.S., and G.P performed  
243 the chemical and isotopic measurements, respectively; All co-authors analyzed data; S.D., wrote  
244 the paper with input from all co-authors.

245 **Funding Sources**

246 This work was supported by the French National CNRS-INSU program LEFE (Les Enveloppes  
247 Fluides et l'Environnement; grant awarded to G.P). D.W. and Z.C. acknowledge financial support  
248 from the Université du Québec à Montréal and the Chinese Academy of Sciences, respectively.

249 **Notes**

250 The authors declare no competing financial interests.

251 **ACKNOWLEDGMENTS**

252 Pavan Datta is acknowledged for organization and on-field support with filter sampling in Delhi,  
253 India. Nathalie Gassama at the University of Tours, France is acknowledged for support with IC  
254 analysis.



255 **REFERENCES**

- 256 1. Thode, H. G. Sulphur isotopes in nature and the environment: an overview. *Stable isotopes:*  
257 *natural and anthropogenic sulphur in the environment* **1991**, *43*, 1-26  
258 [https://scope.dge.carnegiescience.edu/SCOPE\\_43/SCOPE\\_43\\_1\\_Chp1.pdf](https://scope.dge.carnegiescience.edu/SCOPE_43/SCOPE_43_1_Chp1.pdf) (accessed  
259 2021.12).
- 260 2. Seinfeld, J. H.; Pandis, S. N. *Atmospheric Chemistry and Physics: From Air Pollution to*  
261 *Climate Change*; John Wiley & Sons, 2016.
- 262 3. *Climate change 2007: The Physical Science basis*; <https://www.ipcc.ch/report/ar4/wg1/> ,  
263 2007.
- 264 4. Kulmala, M.; Riipinen, I.; Sipilä, M.; Manninen, H. E.; Petäjä, T.; Junninen, H.; Dal Maso,  
265 M.; Mordas, G.; Mirme, A.; Vana, M.; Hirsikko, A. Toward direct measurement of  
266 atmospheric nucleation. *Science* **2007**, *318*, 89-92.
- 267 5. Mertes, S.; Galgon, D.; Schwirn, K.; Nowak, A.; Lehmann, K.; Massling, A.; Wiedensohler,  
268 A.; Wieprecht, W. Evolution of particle concentration and size distribution observed  
269 upwind, inside and downwind hill cap clouds at connected flow conditions during  
270 FEBUKO. *Atmos. Environ.* **2005**, *39*, 4233–4245.
- 271 6. Arias, P.; Bellouin, N.; Coppola, E.; Jones, R.; Krinner, G.; Marotzke, J.; Naik, V.; Palmer,  
272 M.; Plattner, G. K.; Rogelj, J.; Rojas, M. *Climate Change 2021: The Physical Science Basis.*  
273 *Contribution of Working Group 14 I to the Sixth Assessment Report of the*  
274 *Intergovernmental Panel on Climate Change; Technical Summary* **2021**.

- 275 7. Nriagu, J. O.; Coker, R. D.; Barrie, L. A. Origin of sulphur in Canadian Arctic haze from  
276 isotope measurements. *Nature* **1991**, *349*, 142-145.
- 277 8. Shen, Y.; Buick, R.; Canfield, D. E. Isotopic evidence for microbial sulphate reduction in  
278 the early Archaean era. *Nature* **2001**, *410*, 77–81.
- 279 9. Farquhar, J.; Bao, H.; Thiemens, M. Atmospheric influence of Earth's earliest sulfur  
280 cycle. *Science* **2000**, *289*, 756-758.
- 281 10. Ding, T.; Valkiers, S.; Kipphardt, H.; De Bievre, P.; Taylor, P.; Gonfiantini, R.; Krouse, R.  
282 Calibrated sulfur isotope abundance ratios of three IAEA sulfur isotope reference materials  
283 and V-CDT with a reassessment of the atomic weight of sulfur. *Geochim. Cosmochim. Acta*  
284 **2001**, *65*, 2433–2437.
- 285 11. Coplen, T. B. Guidelines and recommended terms for expression of stable-isotope-ratio and  
286 gas-ratio measurement results. *Rapid Comm. Mass Spec.* **2011**, *25*, 2538–2560.
- 287 12. Ono, S.; Wing, B.; Johnston, D.; Farquhar, J.; Rumble, D. Mass-dependent fractionation of  
288 quadruple stable sulfur isotope system as a new tracer of sulfur biogeochemical cycles,  
289 *Geochim. Cosmochim. Acta* **2006**, *70*, 2238–2252.
- 290 13. Dauphas, N.; Schauble, E. A. Mass fractionation laws, mass independent effects, and  
291 isotopic anomalies. *Ann. Rev. Earth Pl. Sci.* **2016**, *44*, 709–783.
- 292 14. Eldridge, D.; Guo, W.; Farquhar, J. Theoretical estimates of equilibrium sulfur isotope  
293 effects in aqueous sulfur systems: Highlighting the role of isomers in the sulfite and  
294 sulfoxylate systems. *Geochim. Cosmochim. Acta* **2016**, *195*, 171–200.

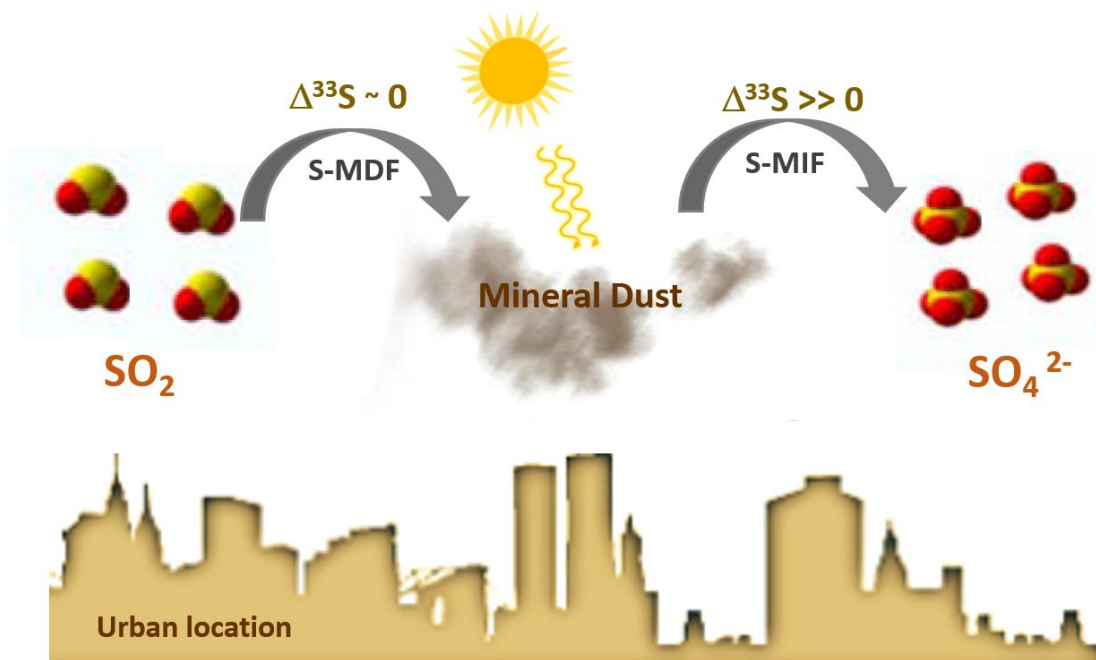
- 295 15. Whitehill, A. R.; Jiang, B.; Guo, H.; Ono, S. SO<sub>2</sub> photolysis as a source for sulfur mass-  
296 independent isotope signatures in stratospheric aerosols. *Atmos. Chem. Phys.* **2015**, *15*,  
297 1843-1864.
- 298 16. Au Yang, D.; Cartigny, P.; Desboeufs, K.; Widory, D. Seasonality in the  $\Delta^{33}\text{S}$  measured  
299 in urban aerosols highlights an additional oxidation pathway for atmospheric SO<sub>2</sub>. *Atmos.*  
300 *Chem. Phys.* **2019**, *19*, 3779-3796.
- 301 17. Lin, M.; Zhang, X.; Li, M.; Xu, Y.; Zhang, Z.; Tao, J.; Su, B.; Liu, L.; Shen, Y.; Thiemens,  
302 M. H. Five-S-isotope evidence of two distinct mass-independent sulfur isotope effects and  
303 implications for the modern and Archean atmospheres. *Proc. Natl. Acad. Sci. U. S. A.* **2018**,  
304 *115*, 8541-8546.
- 305 18. Harris, E.; Sinha, B.; Hoppe, P.; Ono, S. High-precision measurements of <sup>33</sup>S and <sup>34</sup>S  
306 fractionation during SO<sub>2</sub> oxidation reveal causes of seasonality in SO<sub>2</sub> and sulfate isotopic  
307 composition. *Environ. Sci. Technol.* **2013**, *47*, 12174–12183.
- 308 19. Dahiya, S.; Myllyvirta, L. Global SO<sub>2</sub> Emission Hotspots Database: Ranking the World's  
309 Worst Sources of SO<sub>2</sub> Pollution. Greenpeace Environment Trust,  
310 [https://www.greenpeace.org/india/en/publication/3951/global-so2-emission-hotspots-](https://www.greenpeace.org/india/en/publication/3951/global-so2-emission-hotspots-database-ranking-the-worlds-worst-sources-of-so2-pollution-2/)  
311 [database-ranking-the-worlds-worst-sources-of-so2-pollution-2/](https://www.greenpeace.org/india/en/publication/3951/global-so2-emission-hotspots-database-ranking-the-worlds-worst-sources-of-so2-pollution-2/)(accessed 2021.12)
- 312 20. Hama, S. M.; Kumar, P.; Harrison, R. M.; Bloss, W. J.; Khare, M.; Mishra, S.; Namdeo, A.;  
313 Sokhi, R.; Goodman, P.; Sharma, C. Four-year assessment of ambient particulate matter  
314 and trace gases in the Delhi-NCR region of India. *Sustain. Cit. Soci.* **2020**, *54*, 102003.

- 315 21. Gurjar, B. R.; Nagpure, A. S. Indian megacities as localities of environmental vulnerability  
316 from air quality perspective. *J. Smart Cities* **2016**, *1*,15-30.
- 317 22. Dasari, S.; Andersson, A.; Bikkina, S.; Holmstrand, H.; Budhavant, K.; Satheesh, S.; Asmi,  
318 E.; Kesti, J.; Backman, J.; Salam, A.; Bisht, D. S. Photochemical degradation affects the  
319 light absorption of water-soluble brown carbon in the South Asian outflow. *Sci. Adv.* **2019**,  
320 *5*, eaau8066.
- 321 23. Han, X.; Guo, Q.; Strauss, H.; Liu, C.; Hu, J.; Guo, Z.; Wei, R.; Peters, M.; Tian, L.; Kong,  
322 J. Multiple sulfur isotope constraints on sources and formation processes of sulfate in  
323 Beijing PM<sub>2.5</sub> aerosol. *Environ. Sci. Technol.* **2017**, *51*, 7794–7803.
- 324 24. Lee, C. W.; Savarino, J.; Cachier, H.; Thiemens, M. Sulfur (<sup>32</sup>S, <sup>33</sup>S, <sup>34</sup>S, <sup>36</sup>S) and oxygen  
325 (<sup>16</sup>O, <sup>17</sup>O, <sup>18</sup>O) isotopic ratios of primary sulfate produced from combustion processes.  
326 *Tellus B* **2002**, *54*, 193–200.
- 327 25. Lin, M.; Zhang, Z.; Su, L.; Hill-Falkenthal, J.; Priyadarshi, A.; Zhang, Q.; Zhang, G.; Kang,  
328 S.; Chan, C. Y.; Thiemens, M. H. Resolving the impact of stratosphere-to-troposphere  
329 transport on the sulfur cycle and surface ozone over the Tibetan Plateau using a cosmogenic  
330 <sup>35</sup>S tracer. *J. Geophys. Res. Atmos.* **2016**, *121*, 439–456.
- 331 26. Fadnavis, S.; Chattopadhyay, R. Linkages of subtropical stratospheric intraseasonal  
332 intrusions with Indian summer monsoon deficit rainfall. *J. of Climate* **2017**, *30*, 5083-5095.
- 333 27. Harris, E.; Sinha, B.; Foley, S.; Crowley, J. N.; Borrmann, S.; Hoppe, P. Sulfur isotope  
334 fractionation during heterogeneous oxidation of SO<sub>2</sub> on mineral dust. *Atmos. Chem. Phys.*  
335 **2012**, *12*, 4867– 4884.

- 336 28. Paris, R.; Desboeufs, K. V.; Formenti, P.; Nava, S.; Chou, C. Chemical characterisation of  
337 iron in dust and biomass burning aerosols during AMMA-SOP0/DABEX: implication for  
338 iron solubility. *Atmos. Chem. Phys.* **2010**, *10*, 4273–4282.
- 339 29. Formenti, P.; Schütz, L.; Balkanski, Y.; Desboeufs, K.; Ebert, M.; Kandler, K.; Petzold, A.;  
340 Scheuven, D.; Weinbruch, S.; Zhang, D. Recent progress in understanding physical and  
341 chemical properties of African and Asian mineral dust. *Atmos. Chem. Phys.* **2011**, *11*, 8231–  
342 8256.
- 343 30. Tian, S. L.; Pan, Y. P.; Wang, Y. S. Size-resolved source apportionment of particulate  
344 matter in urban Beijing during haze and non-haze episodes. *Atmos. Chem. Phys.* **2016**, *16*,  
345 1-19.
- 346 31. Lin, M.; Biglari, S.; Zhang, Z.; Crocker, D.; Tao, J.; Su, B.; Liu, L.; Thiemens, M. H.  
347 Vertically uniform formation pathways of tropospheric sulfate aerosols in East China  
348 detected from triple stable oxygen and radiogenic sulfur isotopes. *Geophys. Res. Lett.*  
349 **2017**, *44*, 5187-5196.
- 350 32. Fadnavis, S.; Müller, R.; Kalita, G.; Rowlinson, M.; Rap, A.; Li, J. L. F.; Gasparini, B.;  
351 Laakso, A. The impact of recent changes in Asian anthropogenic emissions of SO<sub>2</sub> on  
352 sulfate loading in the upper troposphere and lower stratosphere and the associated radiative  
353 changes. *Atmos. Chem. Phys.* **2019**, *19*, 9989-10008.
- 354 33. Fadnavis, S.; Sabin, T. P.; Roy, C.; Rowlinson, M.; Rap, A.; Vernier, J. P.; Sioris, C. E.  
355 Elevated aerosol layer over South Asia worsens the Indian droughts. *Sci. Rep.* **2019**, *9*, 1-  
356 11.

- 357 34. Paulot, F.; Paynter, D.; Ginoux, P.; Naik, V.; Horowitz, L.W. Changes in the aerosol direct  
358 radiative forcing from 2001 to 2015: observational constraints and regional  
359 mechanisms. *Atmos. Chem. Phys.* **2018**, *18*, 13265-13281.
- 360 35. Guo, Z.; Li, Z.; Farquhar, J.; Kaufman, A. J.; Wu, N.; Li, C.; Dickerson, R. R.; Wang, P.  
361 Identification of sources and formation processes of atmospheric sulfate by sulfur isotope  
362 and scanning electron microscope measurements. *J. of Geophys. Res. Atmos.* **2010**, *115*,  
363 D00K07.
- 364 36. Mast, M. A.; Turk, J. T.; Ingersoll, G. P.; Clow, D. W.; Kester, C. L. Use of stable sulfur  
365 isotopes to identify sources of sulfate in Rocky Mountain snowpacks. *Atmos. Environ.* **2001**,  
366 *35*, 3303–3313.
- 367 37. Philippot, P.; van Zuilen, M.; Rollion-Bard, C. Variations in atmospheric sulphur chemistry  
368 on early Earth linked to volcanic activity. *Nat. Geosci.* **2012**, *5*, 668–674.

*SO<sub>2</sub> Photo-oxidation on mineral dust surface generates S-MIF*



Sulfur Mass-Dependent Fractionation : S-MDF  
Sulfur Mass-Independent Fractionation : S-MIF